Acronyms

ANS American Nuclear Society

BWR boiling water reactor

CASL Consortium for Advanced Simulation of Light Water Reactors

CFL Courant Friedrichs Lewy

CHF critical heat flux

DBA design basis accident

DFFB dispersed flow film boiling

FEBA Flooding Experiments with Blocked Arrays

FFRD fuel fragmentation, relocation, and dispersal

HPC high-performance computing

HT heat transfer

IAFB inverted annular film boiling

INL Idaho National Laboratory

LBLOCA large-break loss-of-coolant accident

LOCA loss-of-coolant accident

LWR light-water reactor

This manuscript has been authored by UT-Battelle, LLC under contract DE-AC05-00OR22725 with the US Department of Energy (DOE). The US government retains and the publisher, by accepting the article for publication, acknowledges that the US government retains a nonexclusive, paid-up, irrevocable, worldwide license to publish or reproduce the published form of this manuscript, or allow others to do so, for US government purposes. DOE will provide public access to these results of federally sponsored research in accordance with the DOE Public Access Plan (http://energy.gov/downloads/doe-public-access-plan).

MFB minimum film boiling

NEAMS Nuclear Energy Advanced Modeling and Simulation

ORNL Oak Ridge National Laboratory

PCT peak cladding temperature

PIRT phenomena identification and ranking table

PNNL Pacific Northwest National Laboratory

PWR pressurized water reactor

T/H thermal hydraulics

USNRC United States Nuclear Regulatory Commission

VERA Virtual Environment for Reactor Applications

Graphical Abstract

A Study on the Impact of Using a Subchannel Resolution for Modeling of Large Break Loss of Coolant Accidents

Robert Salko, Aaron Wysocki, Belgacem Hizoum, Nathan Capps

The nuclear industry is investigating the feasibility of moving from 18- to 24-month fuel cycles because of the positive impact it would have on the operational costs for the current fleet of light-water reactors. A challenge to making this change is the increased risk of fuel fragmentation, relocation, and dispersal (FFRD) due to the known potential of ceramic fuel to pulverize into fine particles at higher-discharge burnups. Previous work has been done by the Nuclear Energy Advanced Modeling and Simulation program to assess FFRD risk in high-burnup cores using the BISON fuel performance code and a coarse mesh thermal hydraulics (T/H) solution for a loss-of-coolant accident (LOCA) using the TRACE system T/H code. Because of the importance of the T/H solution for FFRD assessment, this study investigated the impact of using higher-fidelity subchannel techniques for modeling of the LOCA transient. CTF was used to model a subregion of a high-burnup core that was depleted by the Virtual Environment for Reactor Applications (VERA) multiphysics core simulator. Both coarse-mesh

and pin-resolved models were created in CTF, and a consistent coarse-mesh TRACE model was also developed to allow for benchmarking the code results. A large-break loss-of-coolant accident (LBLOCA) reflood transient was simulated using these three models, and results were compared. Results show some consistent differences between CTF and TRACE coarse models, including a higher peak cladding temperature (PCT) prediction in CTF and later quenching in CTF; however, the transient clad temperature behavior was similar, and these differences are likely due to post-critical heat flux heat transfer modeling differences and minimum film boiling temperature model differences. The pin-resolved results indicate that the PCT in the lumped model is often under-predicted by as much as 70 °C and that the location of PCT for this model is different from the high-power pin in the assembly. The lumped model predicts a difference of 10 °C or less between the average and hot pins in the assembly, whereas the pin-resolved model predicts a range of over 100 °C. These results indicate that higher-fidelity T/H results may have an impact on predicted core behavior during LOCA, which may be important to consider when assessing FFRD risk.

Highlights

A Study on the Impact of Using a Subchannel Resolution for Modeling of Large Break Loss of Coolant Accidents

Robert Salko, Aaron Wysocki, Belgacem Hizoum, Nathan Capps

- Fuel performance depends on thermal hydraulic behavior during severe accidents
- The impact of using subchannel methods to predict loss-of-coolant behavior was investigated
- Using higher fidelity methods allows for a more accurate determination of clad surface temperature behavior

A Study on the Impact of Using a Subchannel Resolution for Modeling of Large Break Loss of Coolant Accidents

Robert Salko[a], Aaron Wysocki[a], Belgacem Hizoum[a], Nathan Capps[a]

[a] *Oak Ridge National Laboratory, One Bethel Valley Road, Oak Ridge, TN, USA*

Abstract

The nuclear industry is investigating the feasibility of transitioning from 18- to 24-month fuel cycles because of the positive impact it would have on the operational costs for the current fleet of light-water reactors. A challenge to making this change is the increased risk of fuel fragmentation, relocation, and dispersal (FFRD) due to the known potential for ceramic fuel to pulverize into fine particles at the higher discharge burnups. Previous work has been performed by the Nuclear Energy Advanced Modeling and Simulation program to assess FFRD risk in high-burnup cores using the BISON fuel performance code and a coarse mesh thermal hydraulics (T/H) solution for a loss-of-coolant accident (LOCA) using the TRACE system T/H code. Because of the importance of the T/H solution for FFRD assessment, this study seeks to investigate the impact of using higher-fidelity subchannel techniques for modeling of the LOCA transient. CTF was used to model a subregion of a high-burnup core that was depleted by the Virtual Environment for Reactor Applications (VERA) multiphysics core simulator. Both coarse-mesh and pin-resolved models were created in CTF, and a consistent coarse-mesh TRACE model was also developed to allow for benchmarking the code results. A large-break loss-of-coolant accident (LBLOCA) reflood transient was simulated using these three models, and results were compared. Results showed some consistent differences between the CTF and TRACE coarse models, including a higher peak cladding temperature (PCT) prediction in CTF and later quenching in CTF; however, the transient clad temperature behavior was similar, and these differences are likely due to post-critical heat flux heat transfer modeling differences and minimum film boiling temperature model differences. The pin-resolved results indicate that the PCT in the

lumped model is often under-predicted by as much as 70 °C and that PCT occurs at a different location than the high-power pin in the assembly. The lumped model predicts a difference of 10 °C or less between the average and hot pins in the assembly, whereas the pin-resolved model predicts a range of over 100 °C. These results indicate that higher-fidelity T/H results may have an impact on predicted core behavior during LOCA, which may be important to consider when assessing FFRD risk.

Keywords: LOCA, subchannel, FFRD

---

1. Introduction

There is interest in the nuclear industry to move from 18- to 24-month fuel cycles because of the potential positive impact on fuel cycle efficiency and operation costs. Increasing the operating length of fuel cycles will, however, push fuel discharge burnup to levels higher than the current operating limit of 62 GWd/tU. One of the concerns with allowing for higher fuel burnup is the increased potential at such burnups of fuel fragmentation, relocation, and dispersal (FFRD) during a loss-of-coolant accident (LOCA). This increased risk is due to the observed tendency during in-pile testing performed at Halden (Fuketa et al. (2010)) and Studsvik (Flanagan et al. (2013)) of the ceramic fuel pellets to pulverize into fine particles that can more easily escape from clad rupture openings as the burnup surpasses 62 GWd/tU. Moving to a 24-month cycle may push the fuel discharge burnups to 75 GWd/tU, thus exceeding this limitation such that FFRD may be a concern (Capps et al. (2022)).

A large-break loss-of-coolant accident (LBLOCA) is one of the most severe accidents that can occur in a light-water reactor (LWR); therefore, FFRD susceptibility must be dispositioned in high-burnup cores. The most limiting LBLOCA in a pressurized water reactor (PWR) is assumed to start when a double-ended guillotine break occurs in the reactor cold leg. This results in a rapid depressurization of the primary coolant loop, flashing of liquid to steam, and uncovering of the core. The cladding begins to heat up due to reduced heat transfer in the voided core, which presents a risk of core damage due to fuel failure.

The LBLOCA progresses in three phases, commonly known as depressurization/blowdown, refill, and reflood. The depressurization phase starts once the break occurs and involves coolant escaping the system and primary

system pressure dropping to containment pressure (i.e., near atmospheric). The refill phase starts when accumulators engage and begin refilling the lower plenum with subcooled liquid. The reflood phase begins once the subcooled liquid begins to fill the core region and quench the hot fuel. The most limiting point of the transient, at which point peak cladding temperature (PCT) is encountered, occurs during the reflood phase. The heat transfer behavior during this phase is complex and challenging to model. Subcooled liquid enters the bottom of the core and quenches the hot fuel as it rises. This quench front produces steam due to evaporation, which rises through the core and causes convective heat transfer. Steam carrying droplets entrained in the quench front serves both to cool the superheated steam at the top of the core and to directly cool the fuel rods; this cooling is achieved through radiative heat transfer and collision with rod surfaces. These effects have been observed in integral LOCA tests such as FLECHT-SEASET (Hochreiter (1985)), FEBA (Ihle and Rust (1984)), and the more recent Rod Bundle Heat Transfer tests (Bajorek and Cheung (2019)).

The PCT in the core is encountered during the reflood phase of the transient. During this phase, several complex and interdependent phenomena, such as droplet entrainment, radiative heat transfer, and spacer grid effects, determine the magnitude of the PCT and the amount of time it takes for the rods to be quenched. The combination of core depressurization, relatively high internal rod pressure, and increasing rod temperatures (reduced mechanical strength of the cladding) can lead to cladding ballooning and rupture, which can lead to dispersal of radioactive fuel particles.

The Nuclear Energy Advanced Modeling and Simulation (NEAMS) program has been investigating the issue of FFRD susceptibility in high-burnup cores, with a focus on identifying margin opportunities. In a previous study on FFRD, RELAP5-3D was used to perform a LBLOCA analysis for a high-burnup core that was modeled by Virtual Environment for Reactor Applications (VERA) (Capps et al. (2021)). The RELAP5-3D results were used as boundary conditions for BISON (Hales et al. (2016)) simulations of limiting rods in the core, which was then used to determine fuel pulverization susceptibility and the likelihood of fuel rod rupture in high-burnup fuel rods. A standard coarse-mesh two-channel/pin modeling approach was used in the RELAP5-3D model in this analysis, which uses one pin/channel to represent limiting rods (high-burnup and high power) and another to represent the remainder of the pins. In another activity, a TRACE model was developed of a four-loop Westinghouse PWR LBLOCA transient (Capps et al. (2022)).

BISON was similarly used to assess high-burnup fuel FFRD susceptibility by analyzing fuel performance figures of merit such as rod internal pressure, fission gas release, PCT, and their relationships between one another and dependencies on core location. The TRACE solution was used to provide boundary conditions for limiting pins modeled by BISON; however, a very coarse radial meshing approach was used that lumps assemblies in the core into five regions. Because of the importance of fuel rod performance gradients on FFRD susceptibility, this study was performed to investigate the impact of significantly increasing the resolution of the thermal hydraulics (T/H) solution so that every pin and coolant channel in the core is explicitly modeled using the CTF subchannel code (Salko et al. (2022)).

An assessment of CTF, which included model validation for LOCA reflood conditions, was performed in previous works (Salko et al. (2023b,c, 2024 (in press)). This previous study also included a sensitivity analysis for LOCA conditions to determine the most important models impacting PCT, quench time, pressure drop, and droplet carryover. The results of this sensitivity analysis were used to guide resource allocation in reviewing closure models impacting LBLOCA results. This paper focuses on scaling the problem size up to the core scale and will use the 3D power distribution predicted from the previously developed high-burnup VERA solution. The reflood portion of the LBLOCA severe accident was modeled using assembly-resolved and pin-resolved strategies in CTF to investigate the impact of using a higher resolution meshing approach. A TRACE model was also created using an assembly-resolved approach, which is higher resolution than previous efforts but still much coarser than the pin-resolved CTF model. This work aimed to make the assembly-resolved TRACE model as consistent as possible with the assembly-resolved CTF model to facilitate code-to-code benchmarking for the selected reflood conditions.

An overview of the CTF and TRACE codes is provided in a preceding paper (Salko et al. (2024 (in press)), but a brief overview is given in Section 2. Section 3 describes the core-scale model and discusses how it was modeled using CTF and TRACE. Section 4 presents the results of both codes and discusses the impact of subchannel resolution modeling for this type of problem. Finally, conclusions are presented in Section 5.

2. Codes

2.1. CTF

CTF is a subchannel T/H code developed by Oak Ridge National Laboratory (ORNL) and North Carolina State University (Salko et al. (2022)); its origins are the COBRA/TRAC code that was developed by Pacific Northwest National Laboratory (PNNL) (Thurgood et al. (1982)). The two-fluid, three-field model, which includes a separate field for modeling the droplet behavior, makes CTF particularly well suited to LBLOCA applications. The code also includes the ability to model cross-flow due to pressure gradients, turbulent mixing, and void drift, and it includes a conduction equation for solving temperature distributions in fuel rods and other solid geometries in the model. The inclusion of pre– and post–critical heat flux (CHF) heat transfer models and flow regime maps allows CTF to be used for both nominal and accident conditions.

A concise summary of the closure models involved in modeling LBLOCA conditions is shown graphically in Figure 1. The major phenomena that must be modeled in these conditions include droplet entrainment and de-entrainment, interfacial heat transfer and drag between the phases—which depends on interfacial area—as well as heat transfer between the rods. Spacer grid effects have also been shown to be important by previous authors (Adams and Clare (1983)); thus, advanced models have been added for consideration of grid quenching and droplet breakup. Under each of these major categories, several sub-models may be required to describe each phenomenon, which are denoted by the next layer of ovals in the diagram.

For example, interfacial effects depend on the flow regime. In addition to the pre-CHF regimes, CTF also considers flow regimes that are unique to post-CHF conditions, such as dispersed flow film boiling (DFFB) and inverted annular film boiling (IAFB). Furthermore, heat transfer from the rod depends on local conditions and may include effects such as radiative heat transfer, boiling, or convective heat transfer. Heat transfer may be enhanced due to spacer grid effects on turbulence and the impact of the droplet field. A more thorough description of the LBLOCA modeling capabilities can be found in an accompanying publication (Salko et al. (2024 (in press)) or the CTF Theory Manual (Salko et al. (2023a)). It is important to note that not all of these models were used in this demonstration because some models have not been adequately assessed or are not feasible to use for core-scale problems at this time. Models that were not enabled for this study include

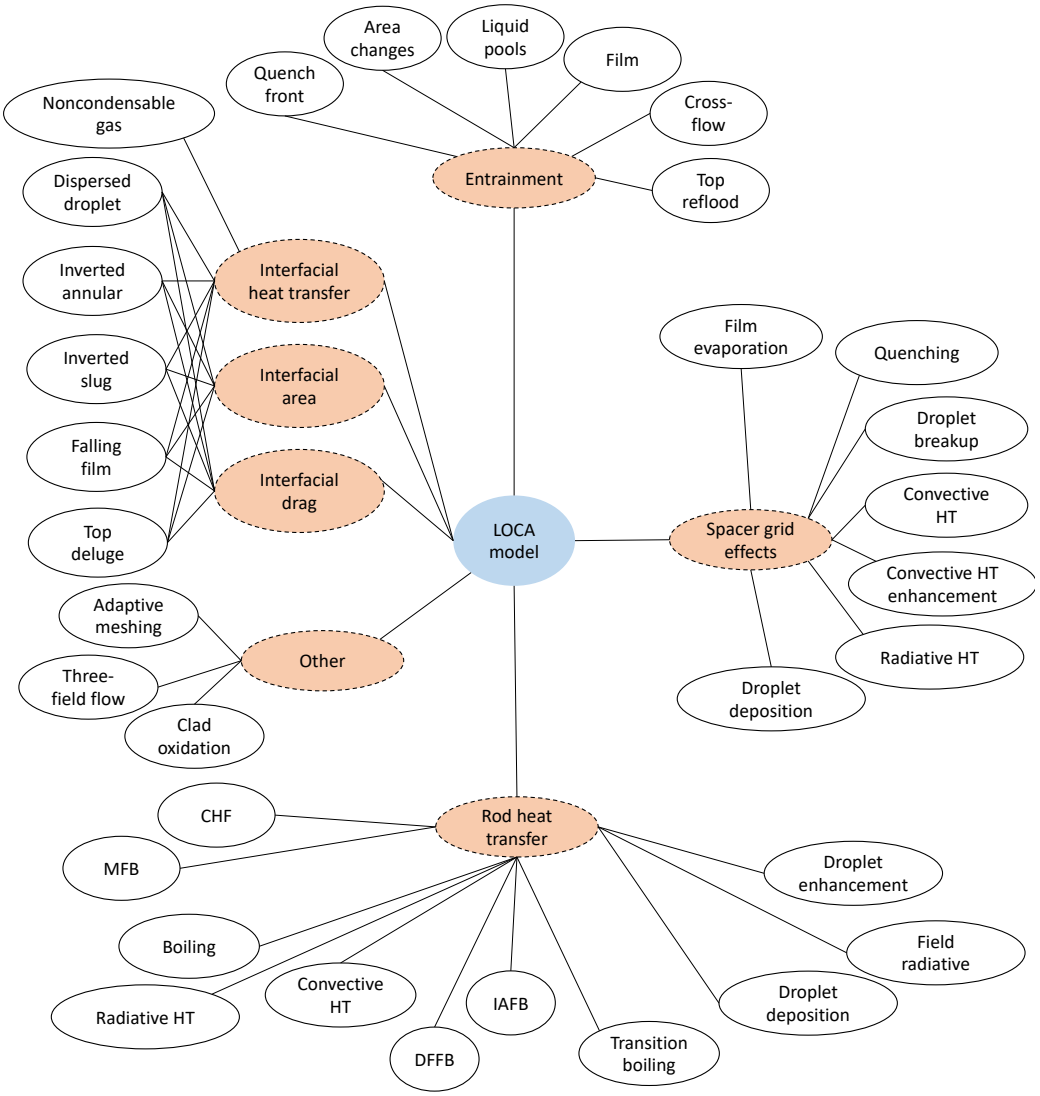

Figure 1: Summary of LOCA reflood phenomena that are considered in CTF.

spacer grid droplet breakup and quenching models, solid-to-solid radiative heat transfer, adaptive meshing of the fuel rods, and clad oxidation.

2.2. TRACE

TRACE is a best-estimate T/H systems code developed by the United States Nuclear Regulatory Commission (USNRC). The capabilities of prior systems codes TRAC-P, TRACE-B, RELAP5, and RAMONA were brought into TRACE as a more modernized computational tool (Bajorek et al. (2015)). TRACE is applicable to a wide range of LWR operational and accident scenarios, including both small and large-break LOCAs. For LBLOCAs, these validation efforts were guided by three LBLOCA-specific phenomena identification and ranking tables (PIRTs) (Shaw et al. (1988); Young et al. (1998); Martin and O'Dell (2005)). These efforts identified the important phenomena that were used to drive the TRACE validation efforts. An independent assessment was performed and concluded that TRACE provides reasonable agreement with these experimental data for LBLOCAs, including correct prediction of LBLOCA trends with minor deficiencies noted in a few constitutive models (Bajorek et al. (2012, 2022a)).

Like CTF, TRACE also solves conservation equations for the liquid and vapor phases separately. However, TRACE does not currently include a separate droplet field equation and lacks some of the more advanced models, such as droplet breakup, spacer grid quenching, and interfacial area tracking. TRACE encounters similar flow regimes and heat transfer regimes, but it uses different models than those of CTF for many of these phenomena, as is later shown. Both codes include IAFB, DFFB, and transition boiling regimes for the post-CHF regime. Considering the extensive validation basis used for assessment of TRACE for LBLOCA conditions, it is useful as a reference point for assessing the CTF solution, which currently lacks the same level of LBLOCA assessment.

3. High-Burnup Core Model

A model of a typical Westinghouse four-loop PWR core containing 193 17×17 assemblies was created and depleted in VERA, as described in a previous study (Capps et al. (2022)). The core design used to achieve 24-month cycles was developed by Southern Nuclear and was provided to ORNL to create a VERA model. Two cycles were used to transition the core from 18-to 24-month cycles and ten cycles were run after that to achieve an equilibrium

pattern. The final cycle resulted in the burnup distribution shown in Figure 2 as predicted by VERA. The VERA prediction of power distribution was used to set the 3D power distribution in the CTF and TRACE models and the burnup distribution was used to set the initial burnup in the pins, which impacts the pellet thermal conductivity and pellet-clad gap thickness.

Because of the small role of neutronics in the reflood transient, a simple time-dependent forcing function was used to simulate the decay heat rather than running a coupled simulation. Furthermore, to reduce the computational expense, a subregion of the full core model was selected for modeling with CTF and TRACE rather than running the full core. This subregion is represented by the black box in Figure 2 and encompasses 9 assemblies of the core. The figure also shows the axial burnup profile of three selected pins in the subregion. One pin is selected from Assembly D-10 and two are selected from E-11. As the figure indicates, there is more variation in pin burnup in the high burnup assemblies. The subregion was selected so as to include both high-burnup and low-burnup assemblies in the region. In this subregion, the center high-burnup assembly is surrounded by both low- and high-burnup assemblies on its faces. While selecting a subregion on the core boundary would include higher burnup assemblies, the power is much lower and would therefore be less interesting from an FFRD risk perspective. The radial power distribution for this subregion at a selected axial location of the model is shown in Figure 3, and the axial power shape of a selected high-burnup rod from the E-10 assembly is shown in Figure 4. At end of cycle, the radial power distribution is relatively uniform in each assembly, but the lower-burnup assemblies are clearly operating at a higher power, and the assembly at the E-11 location is operating at a significantly lower power than other high-burnup assemblies because it is surrounded by high-burnup assemblies.

To perform the assessment, three different models were created for this subregion: a coarse radial mesh TRACE model, a coarse radial mesh CTF model, and a radial fine mesh (pin-resolved) CTF model. The coarse radial mesh models use one channel per assembly in the model, resulting in a total of 9 channels. The channels are connected laterally, allowing for pressure-directed cross-flow and turbulent mixing between the assemblies. Three pins were modeled in each assembly: one pin is the highest power pin in the assembly, the second pin is a lumped, representative pin, which represents the average power in all of the other fuel elements in the assembly, and the third pin is a lumped, representative pin used to represent the guide tubes.

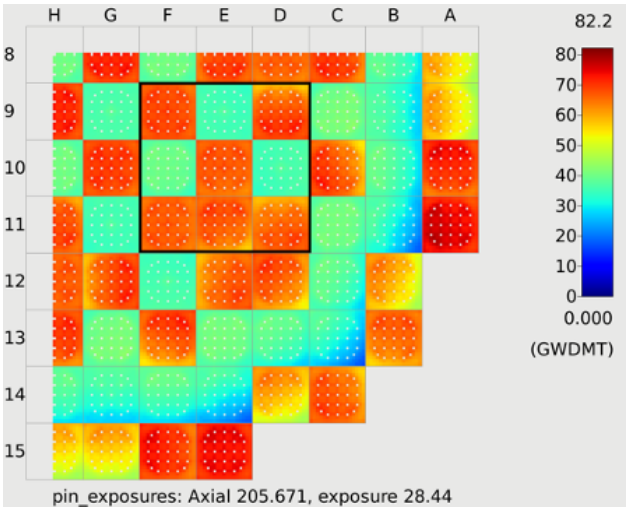

(a) Radial core burnup distribution.

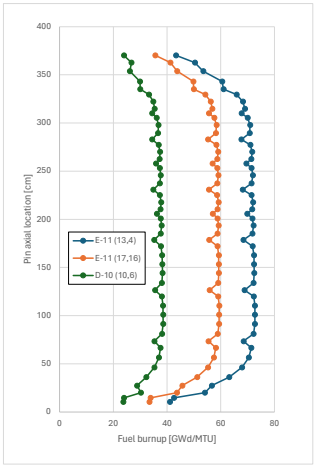

(b) Axial burnup distribution in selected pins.

Figure 2: Core burnup distribution at end of cycle.

Therefore, the hot pin represents only one pin—that with the highest average power in the assembly. The lumped fuel pin represents the other 263 pins in the assembly and uses the averaged axial power shape of those pins. The guide tube pin represents the 25 guide tubes in the assembly. All of these pins connect to the flow channel that represents the assembly in which they reside. In this way, the total power is conserved between coarse and resolved models, but modeling fidelity is lost in the coarse model due to the lumping of the pins and channels. This results in a total of 27 pins in the coarse models. The pin-resolved model resolves each subchannel and pin explicitly using a coolant-centered approach, resulting in a total of 2,704 subchannels and 2,601 pins. Cross-flow connections were set up between each subchannel, and each pin connects to four subchannels.

All three models use the same axial mesh for the fluid, which contains 25 uniform axial levels. The core height is 3.658 m, resulting in axial levels of 0.146 m high. The TRACE model enables fine-mesh renodalization for the pins, which results in the pin axial mesh being refined relative to the fluid axial mesh, particularly in the vicinity of the quench front, to allow for a more accurate solution. CTF also includes this feature, but it was not suitably tested in time for this demonstration, so it was not enabled. The fuel rods are meshed with 10 radial nodes in the pellet region and two nodes in the clad region (one for the inner surface and one for the outer surface). The

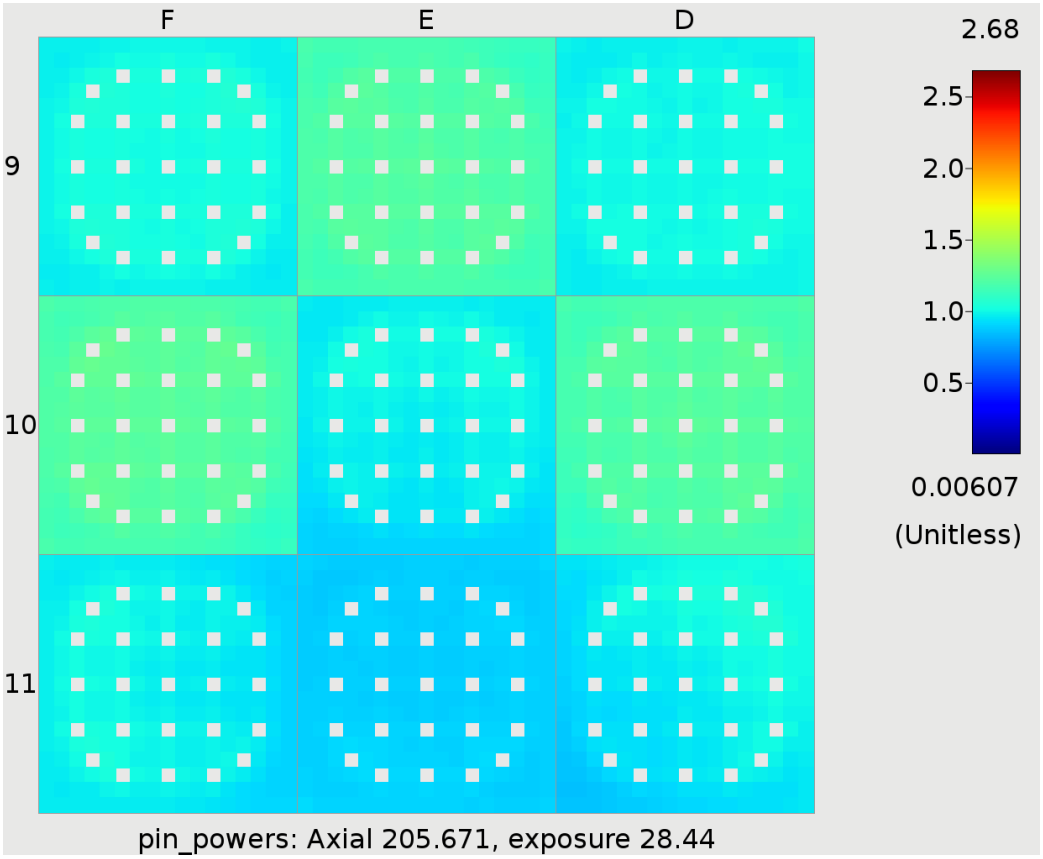

Figure 3: Peaking factor distribution in the high-burnup core subregion at end of cycle.

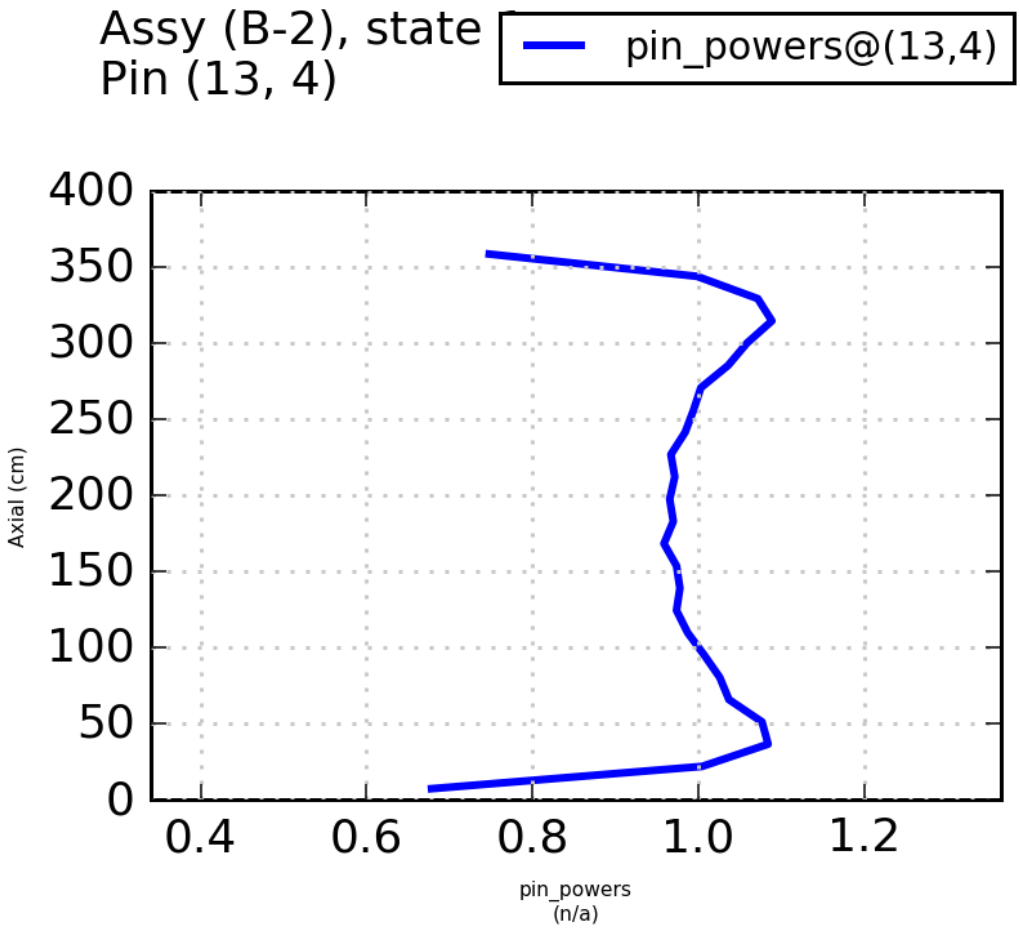

Figure 4: Axial power distribution in high-burnup pin in Assembly E-10.

dynamic gap conductance model is enabled in both codes, which accounts for changes to pellet/clad gap thickness due to thermal expansion and pressure differences between the inside and outside of the fuel rod.

In the CTF models, the turbulent mixing model uses a fixed single-phase mixing coefficient of 0.037, which is the default value for nominal PWR and boiling water reactor (BWR) cases. The Beus model is used to account for two-phase mixing effects, and the void drift model is disabled. Table 1 provides a summary of the wall heat transfer and entrainment models used in CTF and TRACE, which have the most significant impact on pin quenching behavior. The CTF Theory Manual (Salko et al. (2023a)) and TRACE manual (Bajorek et al. (2022b)) contain more detailed descriptions of each of these models and their implementation details. In the table, "Not enabled" indicates that the code has a model for the effect, but it was not used for this study. "Not modeled" means that no model is available for the effect in the code. "See manual" indicates that the model is custom-derived for implementation into the code and, therefore, there is no other author to cite. While some models like the spacer grid models in CTF may have a significant impact on PCT prediction in the core, assessment of these models was not sufficient at the time of this publication to include them in the demonstration. The solid radiative heat transfer will likely also play an important part in equalizing radial temperature distribution, but in addition to not being assessed at this point, the model also cannot be enabled in the CTF preprocessor yet, which would make building a large model impractical.

Table 1: Modeling selections for the high-burnup reflood case

Model parameter	CTF	TRACE
Wall heat transfer models		
CHF	Groeneveld lookup tables	Groeneveld lookup tables
MFB	Modified Berenson	Groeneveld-Stewart
Liquid convection	Dittus-Boelter	Gnielinski
Subcooled boiling	Chen	Saha-Zuber
Saturated boiling	Chen	Gorenflo
Transition boiling	Bjornard and Griffith	Bjornard and Griffith

Continuation of Table 1

Model parameter	CTF	TRACE
Fluid radiative heat transfer	Sun, Dix, and Tien	Hammouda, Groeneveld, and Cheng (IAFB); Sun, Gonzalez, and Tien (DFFB)
Solid radiative heat transfer	Not enabled	Not enabled
Vapor convection	Dittus-Boelter or Wong and Hochreiter	Gnielinski
Droplet turbulence heat transfer enhancement	Kays	Not modeled
Grid spacer heat transfer enhancement	Yao, Hochreiter, and Leech	Yao, Hochreiter, and Leech
Droplet impingement heat transfer	See manual	Not modeled
	Droplet behavior	
Droplet field	Explicit three-field modeling with interfacial area transport equation solution	Explicit droplet transport equations were not enabled; droplet effects are incorporated into the interfacial drag, interfacial heat transfer, and wall heat transfer models
Quench front entrainment	Kataoka, Ishii, and Mishima	Not modeled
Annular film entrainment	Wurtz	Kataoka, Ishii, and Mishima
Film de-entrainment	Cousins	Kataoka, Ishii, and Mishima

Continuation of Table 1

Model parameter	CTF	TRACE
Area-change de-entrainment	Not enabled	Not modeled
Falling film sputtering entrainment	See manual	Not modeled
Spacer grid models		
Grid droplet breakup	Not enabled	Not enabled
Grid quenching model	Not enabled	Paik, Hochreiter, Kelly, and Kohrt
Grid droplet entrainment	Not enabled	Not modeled
Grid/rod radiative heat transfer	Not enabled	Paik, Hochreiter, Kelly, and Kohrt

This demonstration models the reflood portion of the LBLOCA transient only. The boundary and initial conditions were selected in a way that attempts to match the fuel rod quenching behavior of the TRACE subregion, core-only model to a previous full-system TRACE model of a four-loop PWR (Capps et al. (2022)). The TRACE full-system model covers the entire transient starting from the break, which includes blowdown, refill, and reflood. The T/H solution at the core boundaries oscillates considerably during the full TRACE transient, which is partly due to numerical oscillations. Rather than attempting to capture these numerical artifacts and pass them as boundary conditions to CTF, a simplified set of boundary conditions was determined, which leads to similar quenching behavior between the full system and core-only models. The inlet velocity was set to a constant value of $3.8\,\mathrm{cm\,s^{-1}}$, which is consistent with that used in a previous validation study of the Flooding Experiments with Blocked Arrays (FEBA) tests and resulted in good code stability (Salko et al. (2023c)). The inlet temperature was also set to be consistent with the FEBA case. The inlet temperature is 53 °C for the first 30 s of the transient, is linearly ramped down to 38 °C over 2 s, and then remains at that value for the remainder of the transient. The outlet pressure was set to the depressurized value of the TRACE system model,

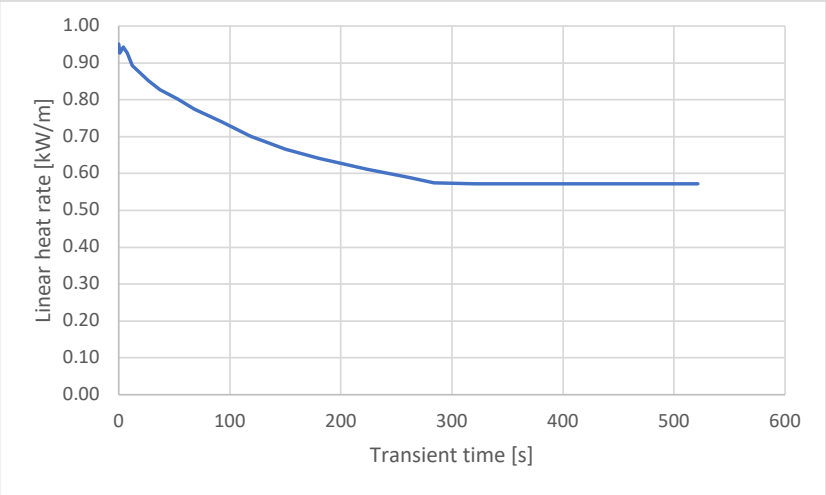

Figure 5: Transient nominal linear heat rate in the high-burnup core during the reflood transient.

which was 2.5 bar. The quench front velocity of the TRACE system model during the reflood portion of the transient actually averaged out to a higher velocity of around $10\,\mathrm{cm\,s^{-1}}$, but this caused pressure spiking in CTF that caused the code to crash. It is believed that this instability is due to the lack of a water packing model Bajorek et al. (2022b) in CTF, which would allow the code to better manage the sudden disappearance of the vapor phase in the control volumes. Lower quench velocities do not pose the same issue as the higher quench velocity case, which is why the lower FEBA value was selected. Because of this consideration, it was necessary to scale the power down so that the PCT profile of the pins remained consistent with the TRACE system model. The rate of power decrease was taken from the FEBA case, but the nominal core power was scaled to obtain a good match of PCT between the TRACE system and core-only models. The transient linear heat rate is shown in Figure 5. Note that this linear heat rate was multiplied by the local pin power factor to obtain the absolute power in that portion of the pin.

The initial void was set to 100 % so that the core would be completely vapor, and the initial velocity was set to zero. The initial temperature distribution in the pin was set using the results of the TRACE full-system model. The TRACE full system model explicitly resolved 321 fuel rods located in different parts of the core in fresh, once-, and twice-burned fuel with consid-

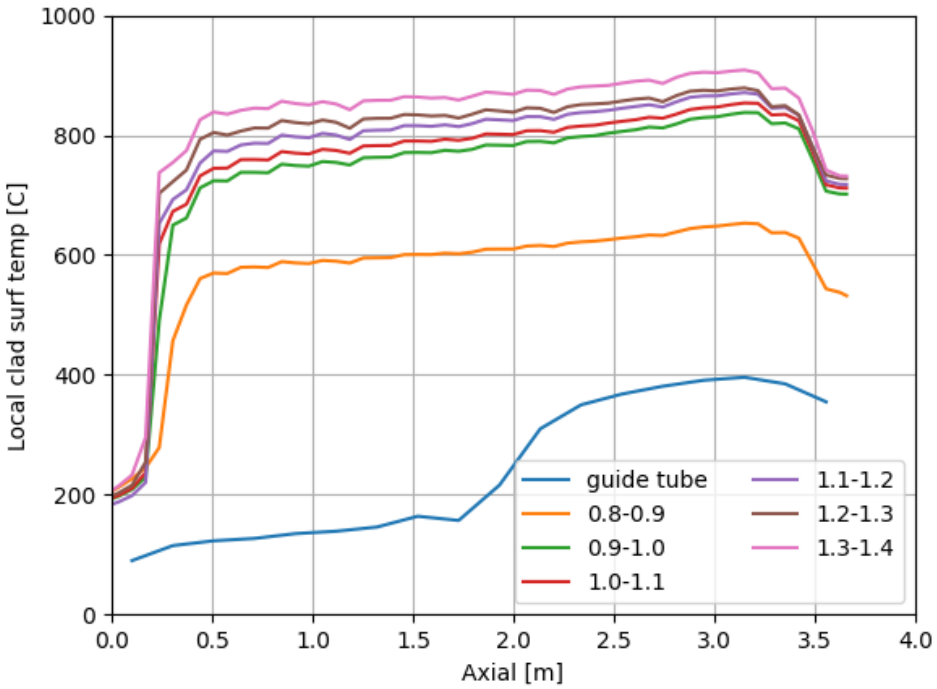

Figure 6: Initial axial clad surface temperature profile for representative pins in specified pin power ranges calculated from TRACE full-system model data.

eration for pin internal pressure and power level. In this way, the behavior of a wide range of fuel pin conditions was captured and used to generate a range of pin temperature responses during the blowdown transient. The average power factor of each of these pins was calculated, and the pins were organized into bins of 0.8–0.9, 0.9–1.0, and so on, up to a power factor of 1.4. The axial clad surface temperature profile of all of the pins in a given power bin was averaged to obtain a single pin axial temperature distribution. This resulted in 6 representative pins and one guide tube, which are shown in Figure 6.

These pin shapes were used to set the initial axial temperature distribution in both the lumped and pin-resolved CTF models by calculating the average pin power of each pin and then selecting the temperature shape associated with that average power. The initial clad surface temperatures of the pins in the pin-resolved model for a selected axial location are shown

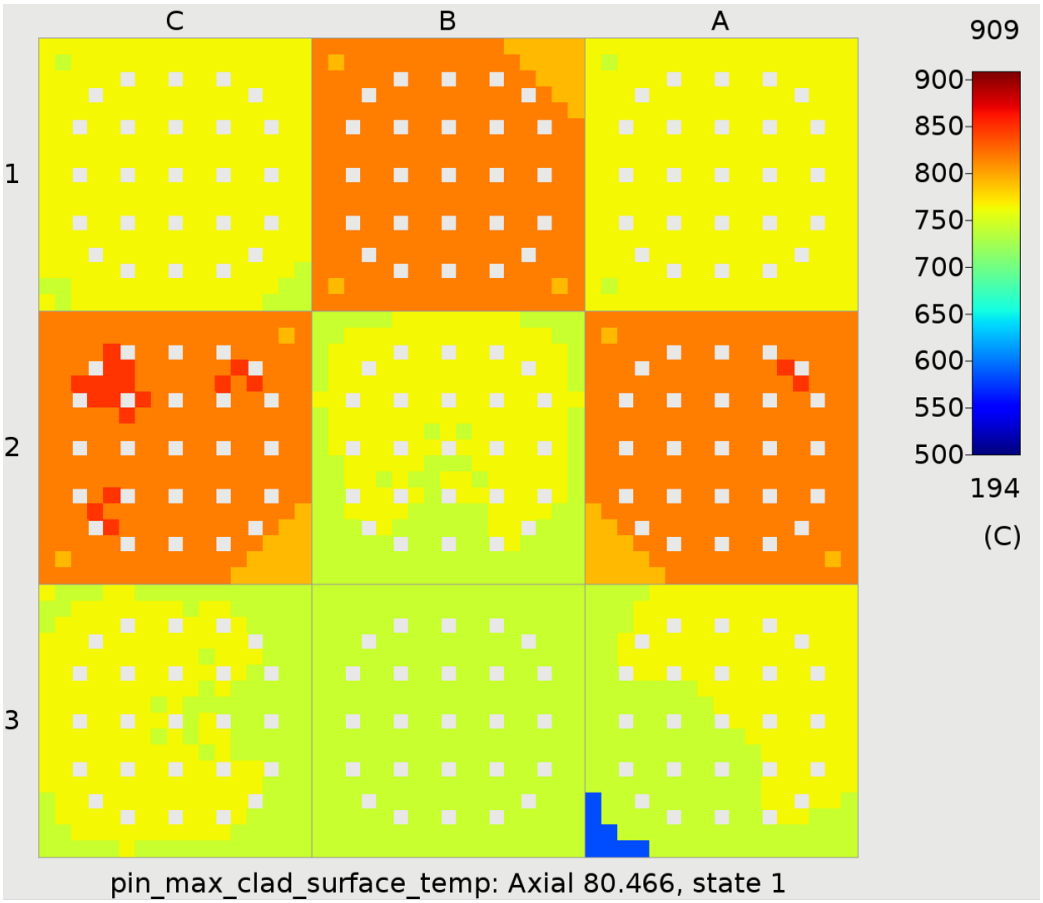

Figure 7: Initial radial surface temperature distribution at selected axial level in the pin-resolved model.

in Figure 7. The availability of only six representative pins led to a fairly coarse initial temperature distribution. Because of the strong impact of initial temperature on PCT in the pin, as is shown later, future work would ideally model the full transient, including blowdown, to obtain a more accurate initial temperature distribution. In CTF, a steady-state calculation was performed for the conduction equation before starting the transient to obtain a radial temperature distribution in the pins. This information was extracted from CTF and was used to initialize the axial and radial power shape in the TRACE lumped model.

4. Results

The cases were run on the Idaho National Laboratory (INL) Sawtooth high-performance computing (HPC) system. The lumped models were run using one processor, whereas the pin-resolved CTF model used 144 processors. The pin-resolved model was run with different maximum allowable timestep sizes to investigate the impact of timestep size on the results. CTF uses an algorithm to control the timestep size that considers the maximum field velocity in the system (Courant Friedrichs Lewy (CFL) limit), maximum pressure change in one timestep, and maximum void change in one timestep. The maximum allowable timestep size is a user input value that prevents the dynamically controlled timestep size from growing larger than a set value. Figure 8 shows the spread of the PCT of all pins in each assembly using box and whisker plots. The figure includes 9 subfigures, each of which provides results for the 9 assemblies in the subregion of the core. Each subfigure shows three box and whisker plots, which correspond to a maximum timestep size of 1×10^{-3} s, 5×10^{-4} s, and 2.5×10^{-4} s.

As the figure indicates, the PCT values normally increase with the smaller timestep size. Although the PCT was observed to continue increasing at the smallest timestep size, it can be seen that the spread of the PCT values does not change substantially between cases, which is one of the important factors when comparing pin-resolved to lumped cases. There was also no trend in the data spread with respect to maximum allowable timestep size, meaning the difference between the lowest PCT pin and highest PCT pin did not continuously decrease or increase as maximum allowable timestep size was decreased. It was found that the maximum change the the data spread (i.e., difference between the highest and lowest PCT pin) for any assembly and timestep size change was 5.9 K. This occurred in Assembly E-9 where the data spread was on the order of 50 K. Therefore, to keep runtime reasonable, a maximum allowable timestep size of 1×10^{-3} s was chosen for the CTF cases. This maximum timestep size was used for both pin-resolved and lumped CTF models. For TRACE, a maximum allowed timestep size of 1×10^{-1} s was imposed. However, due to the TRACE internal timestep control algorithm, which limits the timestep size due to numerical accuracy considerations, the actual largest timestep achieved during the event was 3.2×10^{-2} s. An additional TRACE runs was performed with a maximum allowed timestep size of 5×10^{-3} s, but the impact on PCT was less than 4 K. Therefore, the TRACE results were assumed to be well-converged in

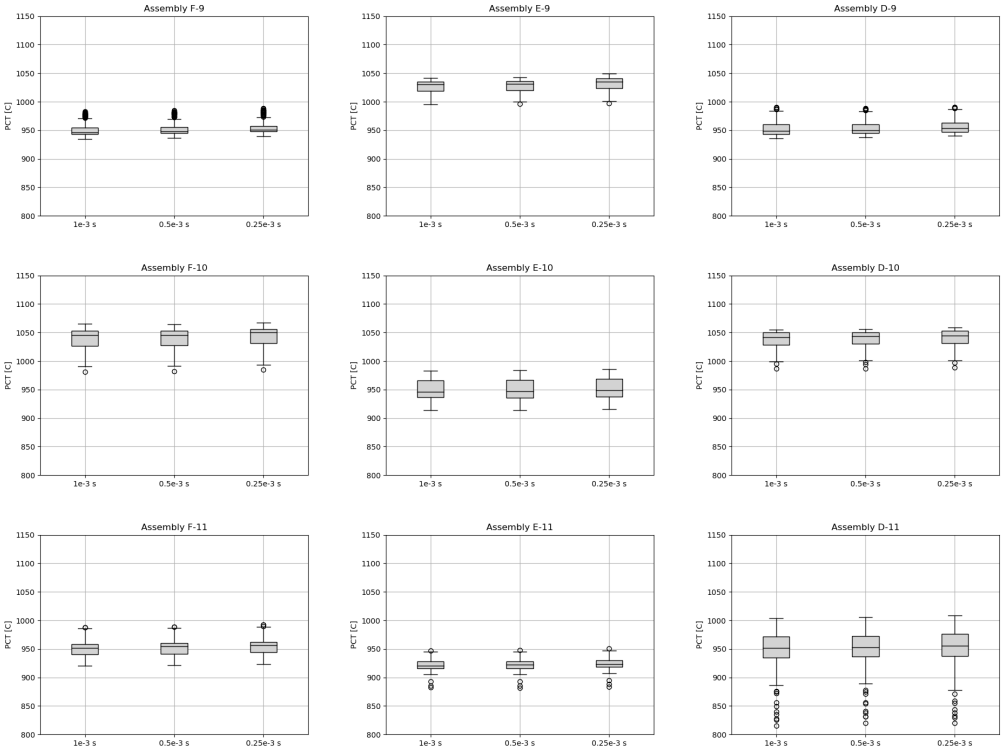

Figure 8: The spread of pin peak cladding temperatures in all assemblies in the pin-resolved subregion model for different maximum allowable timestep sizes.

terms of timestep size.

The transient PCT behavior of the hot pins in the 9 assemblies is shown in Figure 9. The TRACE PCT data, which are represented by the blue lines, are shown for the axial location where maximum PCT occurs in the hot pin. The solid line shows the high-power pin behavior, and the dashed line shows the average pin behavior. The axial location where PCT occurs changes between assemblies. The value in parentheses in the legend denotes the axial location where PCT occurs in the high-power pin for that assembly in units of meters. The CTF lumped data are shown for high-power and average pins using the red solid and dashed lines, respectively. Like the TRACE data, the axial location where PCT occurs in the high power pin is shown. The spread of the pin clad surface temperatures in the resolved model is shown with the shaded green region. The axial location where PCT occurred in the lumped CTF high power pin is used for pin-resolved data. The lower boundary of

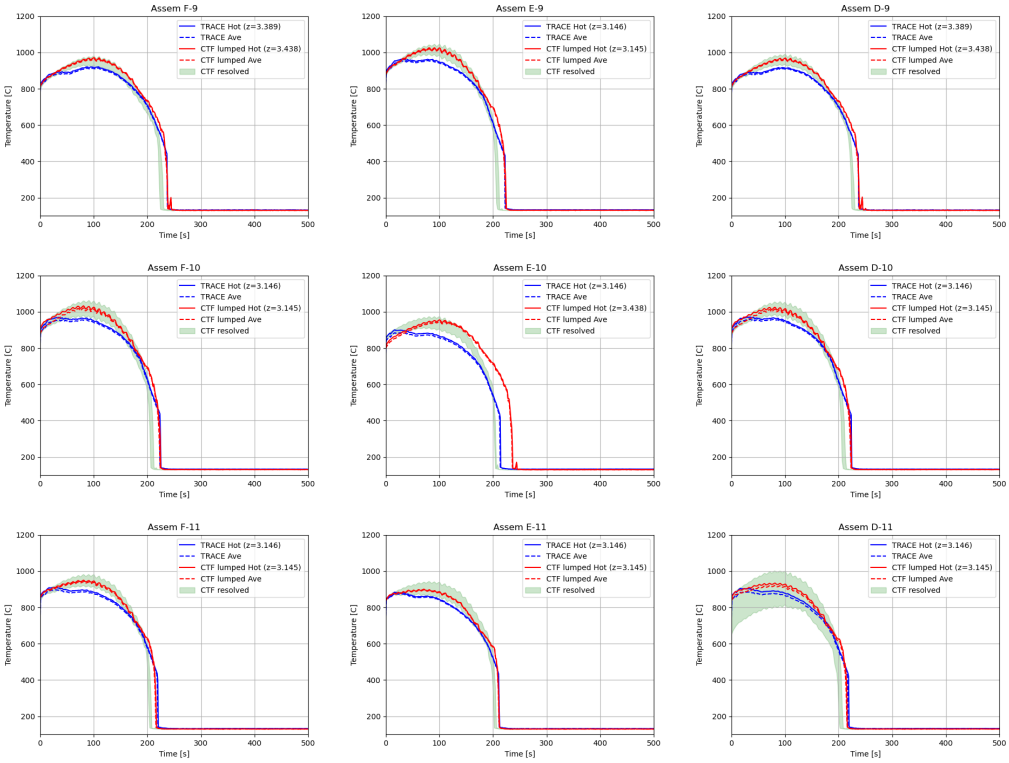

Figure 9: Transient peak cladding temperature behavior of the three models in each of the 9 assemblies of the subregion.

the shaded region represents the lowest fuel rod clad surface temperature, and the upper boundary of the shaded region represents the highest fuel rod clad surface temperature for a given timestep. Therefore, all pin clad surface temperatures for that timestep will fall somewhere between the lower and upper bounds.

To further examine the distribution of pin temperatures, the PCT of every pin, regardless of the axial location, is shown as a histogram for each assembly in Figure 10. In addition to the PCT distribution, the lumped average and hot pin PCT are shown as black and red vertical lines, respectively. The lumped model PCT results always fall within the range of the pin-resolved results; however, the difference between lumped average and hot pin PCT is normally quite small compared to the range of the pin-resolved results. The hot pin is typically within 10 °C of the average pin in the lumped model, whereas the range in PCT of the pin-resolved model is usually around 50 °C,

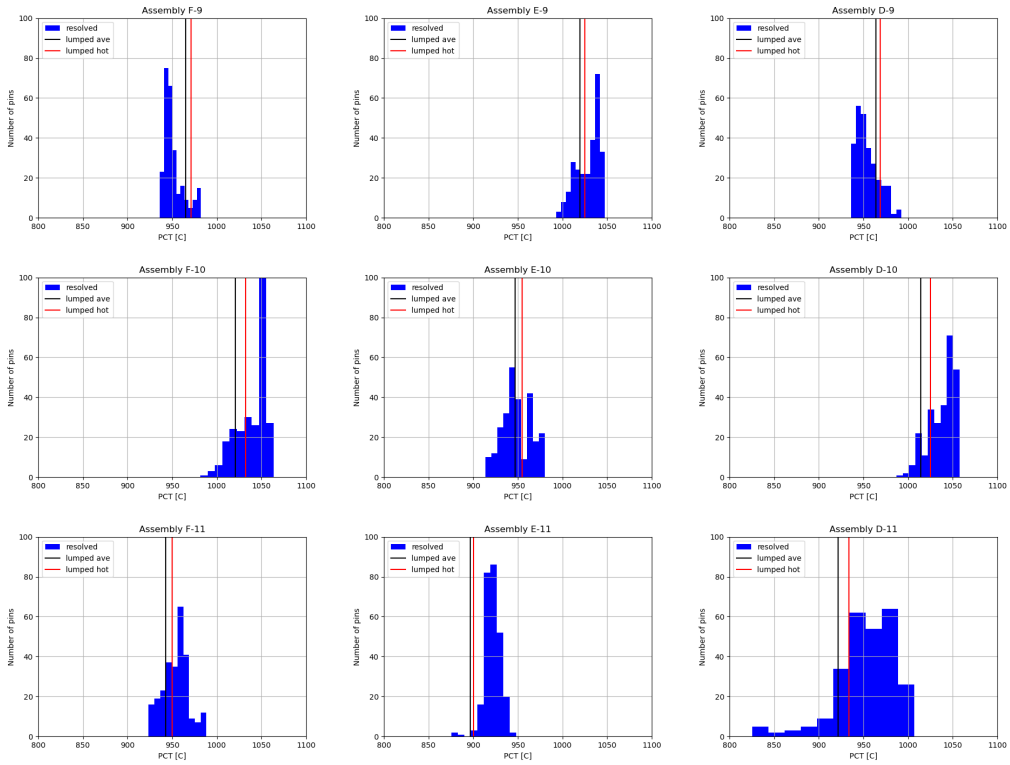

Figure 10: Distribution of peak cladding temperature in every pin for each of the 9 assemblies with black and red vertical lines denoting the average and hot-pin peak cladding temperature in the lumped CTF model.

but sometimes over 150 °C. The low-burnup assemblies in particular see the majority of pins having their PCT under-predicted compared to the pin-resolved model. Some high-burnup assemblies see a significant number of pins as having a lower PCT than the average pin in the lumped model.

A few conclusions can be drawn from these results:

1. The PCT of the CTF lumped model is always within the bounds of the pin-resolved results.
2. PCT is always higher in the pin-resolved model, which is likely due to local T/H effects. The hot pin in the lumped model is transferring heat to a single, lumped channel, which will have a lower enthalpy than the hot subchannels in the pin-resolved model, leading to lower PCT values. This finding demonstrates that the coarse mesh method will typically under-estimate PCT.

3. The CTF lumped model always achieves a higher PCT than the TRACE model, sometimes by as much as 100 °C. Note that the PCT prediction for the FEBA validation cases that were previously run (Salko et al. (2023c)) indicate much better agreement between CTF and TRACE. These results indicate that predicted heat transfer behavior is very closely tied to LOCA boundary and initial conditions and that differences between the post-CHF models clearly exist in the two codes.
4. The pin-resolved model captures pins with a lower PCT than the average pins in the lumped models, which is again due to local T/H effects. This behavior is pronounced for Assembly D-11, which had a more varied set of initial temperatures than other assemblies. This indicates a need to expand the assessment to full core and include the blowdown phase in the CTF model to more accurately capture the initial pin temperature distribution at start of reflood. One potential objective of performing a higher resolution simulation is to identify pins that fall below the burst limitation for high-burnup pins, which would result in a margin gain for a high-burnup core.

To show the location of the assembly PCTs, Figure 11 presents the cladding surface temperature distribution for the axial level where maximum PCT occurs during the transient. As the figure shows, the hottest pins in the high-burnup assemblies tend to be located near the boundary of the assembly next to lower-burnup, higher-power assemblies. Figure 12 shows a close-up view of the center high-burnup assembly (E-10) cladding surface temperature distribution. The figure also shows the location of the high-power pin (black square) that was used as the hot-pin in the lumped model, as well as the highest temperature pin (black circle) in the pin-resolved model. This shows that the PCT pin may be shifted away from the the highest power pin in the assembly due to local T/H and cross-flow effects caused by the adjacent higher-power assembly. This behavior was observed in the other high-burnup assemblies as well. In the case of Assembly E-10, the cladding temperature is 34 °C higher than the the temperature of the high-power pin, and it is 20 °C higher than the hot pin PCT in the lumped CTF model. The low-burnup assemblies are also affected by neighboring assemblies and local T/H. Figure 13 shows the clad surface temperature distribution in Assembly D-10, which is the low-burnup assembly to the right of E-10. In this case, the PCT occurs in the middle row of the assembly and is shifted close to the right boundary. There is no cross-flow on the right edge of the assembly, so

Table 2: Comparison of pin-resolved PCT with pin-resolved high-power pin PCT and lumped model hot pin (difference from maximum pin-resolved PCT value shown in parentheses).

Assembly	Location	Pin-resolved PCT [°C]		Lumped PCT [°C]
		Max	High-power pin	High-power pin
F-9	(13, 4)	982	947 (−35)	971 (−11)
E-9	(4, 13)	1047	1034 (−13)	1025 (−22)
D-9	(14, 13)	992	943 (−49)	968 (−24)
F-10	(5, 4)	1064	1058 (−6)	1032 (−32)
E-10	(13, 4)	980	941 (−39)	955 (−25)
D-10	(14, 5)	1058	1052 (−6)	1025 (−33)
F-11	(4, 5)	988	960 (−28)	950 (−38)
E-11	(5, 14)	948	913 (−35)	900 (−48)
D-11	(13, 4)	1007	973 (−34)	934 (−73)

it acts as an adiabatic boundary condition and leads to the highest temperatures occurring in this location. Although the pin at (14, 5) is the highest power pin, it is 6 °C cooler than the highest temperature pin at location (17, 14). A summary of the limiting pins is provided in Table 2 for all 9 assemblies. The table presents the location of the high power pin in the lattice (given as column, row), maximum PCT and the PCT of the highest average power pin in the pin-resolved model, and the PCT of the highest average power pin in the lumped model. In parentheses, the difference between the PCT of the high-power pin and the true maximum PCT in the pin-resolved model is provided. The reader should note that the radiative heat transfer model was not enabled in this study because a thorough assessment of that model has not yet been completed. Enabling this model will likely increase the heat transfer between the hot low-burnup assemblies and cooler high-burnup assemblies, thus further increasing PCT of the boundary pins in the high-burnup assemblies.

One final comment about these results pertain to the impact of uncertainty on results. The uncertainty of the underlying closure models as well as core operating conditions will lead to uncertainty in the predicted PCT. Quantifying this uncertainty requires a rigorous study to determine input uncertainty distributions for the many models impacting LOCA conditions and is out of scope for this study. While the true accuracy of these predictions cannot be quantified without uncertainty bounds on the results, observations

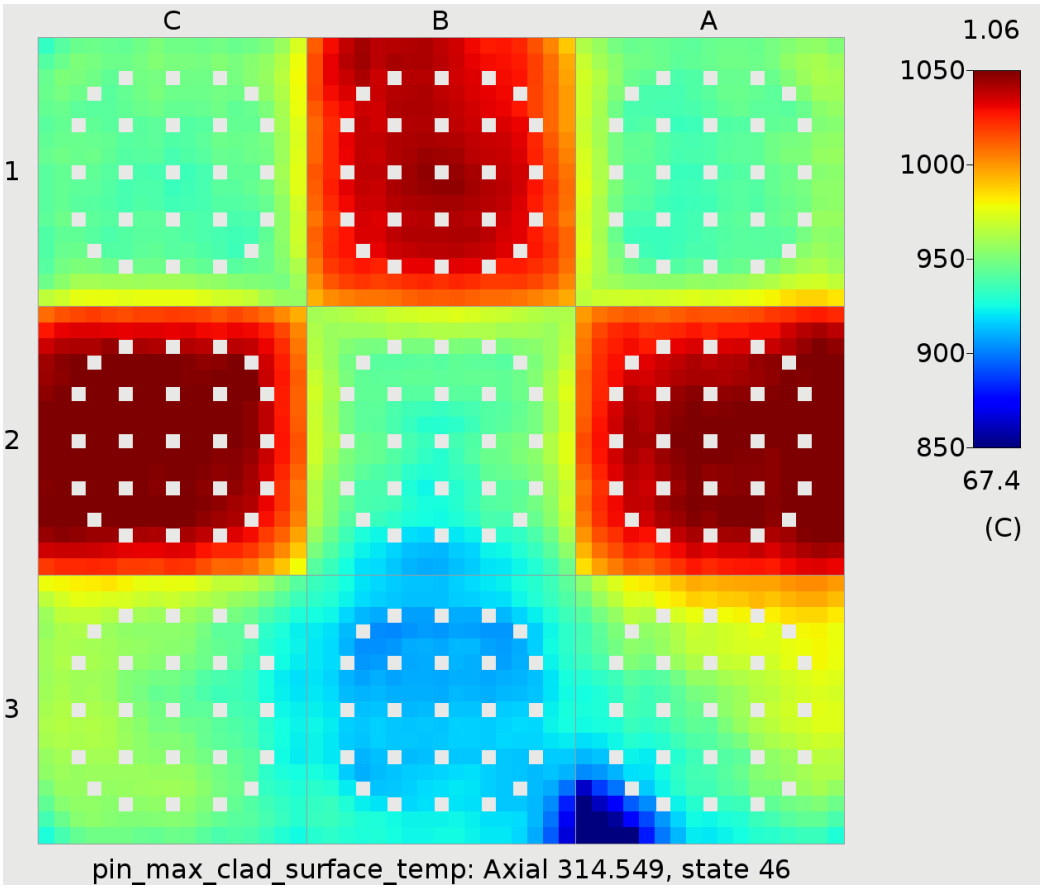

Figure 11: Cladding surface temperature distribution in the pin-resolved model at the axial location where maximum peak cladding temperature occurs.

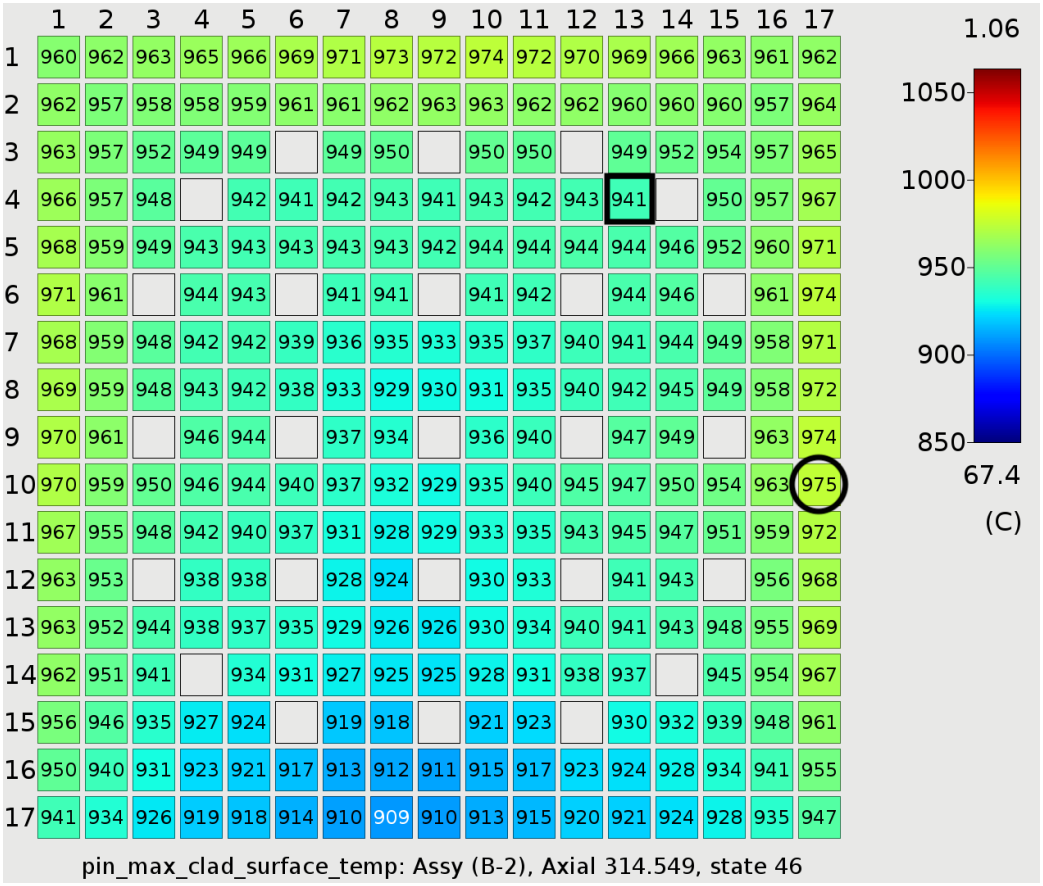

Figure 12: Cladding surface temperature distribution in the pin-resolved model of Assembly E-10 at the axial location where core PCT occurs. The black square shows the pin with the highest average power, and the black circle shows the pin with the highest clad surface temperature.

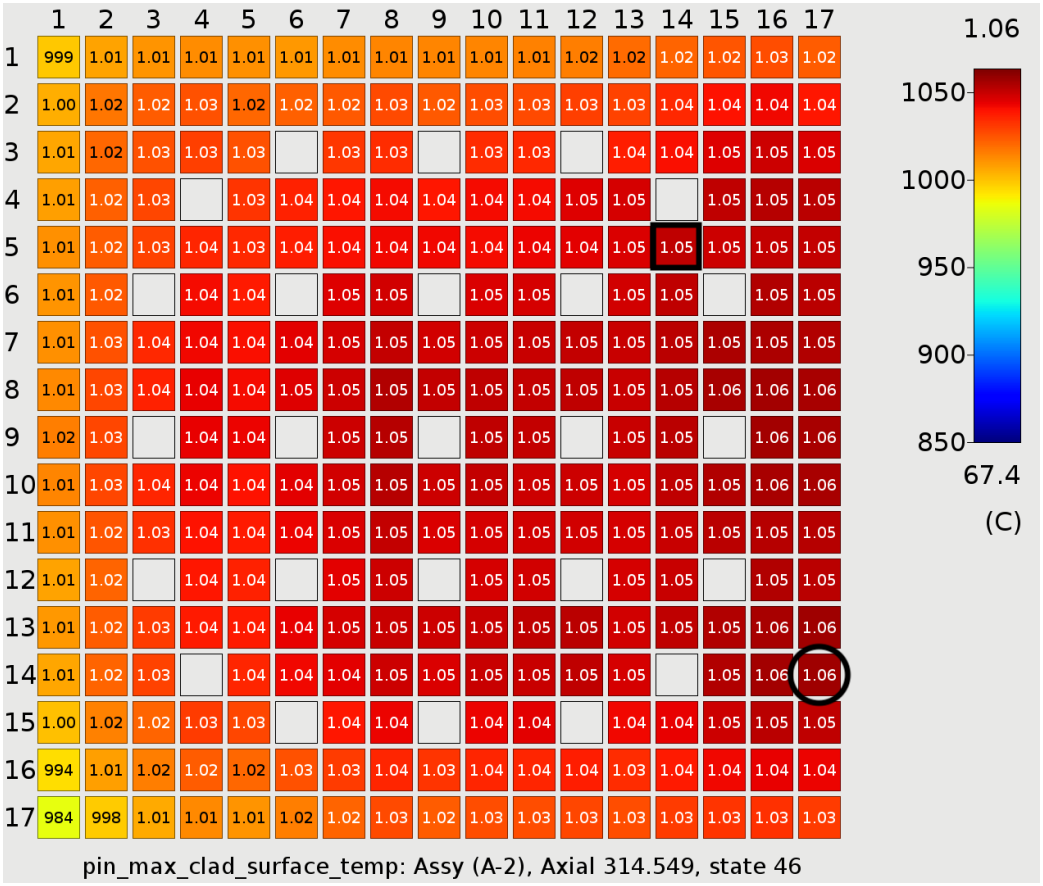

Figure 13: Cladding surface temperature distribution in the pin-resolved model of Assembly D-10 at the axial location where core PCT occurs. The black square shows the pin with the highest average power, and the black circle shows the pin with the highest clad surface temperature.

may be made related to the impact of using a subchannel meshing approach compared to a coarse-mesh approach, as the same models are used in both cases. Furthermore, pins in different regions of the model will experience similar quenching behavior and encounter the same closure models for predicting that behavior.

5. Conclusion

The nuclear industry is interested in increasing fuel cycle length from 18 to 24 months to increase the economic of nuclear power generation. However, there is possibly an increased risk of FFRD as discharge burnup of the fuel is increased to values as high as 75 GWd/tU or higher. The NEAMS program is investigating FFRD in high-burnup cores using its suite of high-fidelity software tools and methods. Previous work in this area has demonstrated the importance of T/H conditions with respect to fuel performance in high-burnup cores using coarser meshing approaches in the T/H methods. This study investigated the impact of using higher fidelity subchannel T/H for modeling of the LBLOCA, which is one of the severe accidents for which FFRD risk will need to be assessed.

A high-burnup core was depleted in VERA to obtain a 3D power distribution at the end of cycle. This was used to create coarse and fine mesh models in CTF and TRACE of a subregion of the core; these models were then subjected to a reflood transient. Results were analyzed and demonstrate the ability of the pin-resolved model to capture a range of clad PCT values in both low- and high-burnup assemblies that were not captured in the lumped model. While the lumped models tried to anticipate the maximum PCT by modeling the highest power pin explicitly, this PCT was always lower than the maximum PCT in the pin-resolved model, which successfully captured local T/H effects as well as cross-flow effects due to adjacent assemblies that have higher or lower decay heat. The pin-resolved model results show that the actual PCT location in the high-burnup assemblies always occurred on the boundary of the assembly when that assembly was adjacent to a low-burnup assembly, which will have a higher decay heat than the high-burnup assembly. Furthermore, low-burnup assemblies also see their actual PCT clad move farther into the assembly because the assembly boundary gives up energy to the higher-burnup neighboring assemblies. Differences between maximum PCT in the pin-resolved model and the high-power pin in the

lumped model were 11–73 °C for the high-burnup assemblies and 22–33 °C for the low-burnup assemblies.

This study indicates that core behavior and clad surface temperature prediction may be impacted by the use of higher fidelity modeling tools over traditional coarse mesh methods by accounting for spatially dependent behaviours (e.g., pin power and pin location). Considering the importance of local T/H behavior for the prediction of fuel performance, it may be necessary to consider more localized effects when assessing FFRD risk. Although this study provides insights into this issue, there is more work that can be done in the future to improve the findings of the study. First, several models in CTF were not yet activated, and their activation in the future will likely have a significant impact on the results. These include models for such phenomena as spacer grid droplet breakup, spacer grid quenching, rod-to-rod and rod-to-grid radiative heat transfer, and rod fine-mesh renodalization. These models should be assessed, validated, and used to perform a similar study in the future. Second, CTF has not yet been assessed for the blowdown phase of the LBLOCA transient; because of this, coarse-mesh TRACE data had to be used to estimate initial clad temperatures. If CTF is used to model the blowdown phase, then a more accurate initial core temperature distribution will be obtained and may lead to a change in the PCT distribution in the assemblies. Furthermore, results for these conditions also indicate that CTF predicts higher PCT than does TRACE, which should be further investigated by expanding on the LBLOCA validation cases used for CTF assessment, as well as potential post-CHF model improvement. While a subregion of the full core was selected for this preliminary analysis, it would be more interesting to perform an analysis of the full core region at subchannel resolution, as this will allow for assessment of the behavior of the higher burnup assemblies on the periphery as well as the larger power gradient near the core edge. Finally, the improved fidelity T/H solution should be used as a boundary condition for the fuel performance code to perform a more thorough FFRD assessment to more fully demonstrate the impact of T/H modeling fidelity on FFRD risk.

Acknowledgments

This research was supported by the Nuclear Energy Advanced Modeling and Simulation program for Modeling and Simulation of Nuclear Reactors under US Department of Energy (DOE) contract no. DE-AC05-00OR22725.

This research made use of Idaho National Laboratory's High Performance Computing systems located at the Collaborative Computing Center and supported by the Office of Nuclear Energy of the U.S. Department of Energy and the Nuclear Science User Facilities under Contract No. DE-AC07-05ID14517.

References

Adams, J., Clare, A., 1983. A Preliminary Study of Droplet Breakup at PWR Spacer Grids. Technical Report. Central Electric Generating Board, PWR/HTWS/P.

Bajorek, S., et al., 2012. TRACE V5.0 Assessment Manual: Main Report. Technical Report ML120060208. United States Nuclear Regulator Commission.

Bajorek, S., et al., 2022a. TRACE V5.0 Developmental Assessment, Addendum 7A: V5.0 Patch 7.

Bajorek, S., et al., 2022b. TRACE V5.0 Patch 7 Theory Manual: Field Equations, Solution Methods, and Physical Models. Technical Report. United States Nuclear Regulator Commission.

Bajorek, S.M., Bernard, M., Gingrich, C., Hoxie, C.L., Ireland, A., Kelly, J., Mahaffy, J., Spore, C., Staudenmeier, J., Thurgood, J.M., Tien, M.K., Whitman, J., 2015. Development, validation, and assessment of the trace thermal-hydraulics systems code, in: NURETH-16, Chicago, IL, August 30–September 4, 2015, pp. 8265–8278.

Bajorek, S.M., Cheung, F.B., 2019. Rod bundle heat transfer thermal-hydraulic program. Nuclear Technology 205, 307–327. doi:10.1080/00295450.2018.1510697.

Capps, N., Hirschhorn, J., Wysocki, A., Greenquist, I., 2022. Assessment of the Effect of Prototypic High-Burnup Operating Conditions of Fuel Fragmentation, Relocation, and Dispersal Susceptibility. Technical Report ORNL/SPR-2022/2597. Oak Ridge National Laboratory.

Capps, N., Wysocki, A., Godfrey, A., Collins, B., Sweet, R., Brown, N., Lee, S., Szewczyk, N., Hoxie-Key, S., 2021. Full core loca safety analysis for a pwr containing high burnup

fuel. Nuclear Engineering and Design 379, 111194. URL: https://www.sciencedirect.com/science/article/pii/S0029549321001461, doi:https://doi.org/10.1016/j.nucengdes.2021.111194.

Flanagan, M., Askeljung, P., Purana, A., 2013. Post-Test Examination Results from Integral High Burnup Fueled LOCA Test at Studsvik Nuclear Laboratory. Technical Report NUREG-2160. US NRC, Office of Nuclear Regulatory and Research.

Fuketa, T., Nagase, F., Grandjean, C., Petit, M., Hozer, Z., Kelppe, S., Khvostov, G., Hafidi, B., Therache, B., Heins, L., Valach, M., Voglewede, J., Wiesenack, W., 2010. Safety Significance of the Halden IFA-650 LOCA Test Results. Technical Report NEA-CSNI-R–2010-5. Nuclear Energy Agency of the OECD (NEA).

Hales, J.D., Williamson, R.L., Novascone, S.R., Pastore, G., Spencer, B.W., Stafford, D.S., Gamble, K.A., Perez, D.M., Liu, W., 2016. BISON Theory Manual The Equations behind Nuclear Fuel Analysis. Technical Report INL/EXT-13-29930. Idaho National Laboratory. doi:10.2172/1374503.

Hochreiter, L.E., 1985. FLECHT SEASET Program Final Report. Technical Report NUREG/CR-4167. Westinghouse Electric Corporation.

Ihle, P., Rust, K., 1984. FEBA—Flooding Experiments with Blocked Arrays Evaluation Report. Technical Report KfK 3657. Institut fur Reaktorbauelemente Projekt Nukleare Sicherheit.

Martin, R.P., O'Dell, L.D., 2005. Areva's realistic large break loca analysis methodology. Nuclear Engineering and Design 235, 1713–1725. URL: https://www.sciencedirect.com/science/article/pii/S0029549305000762, doi:https://doi.org/10.1016/j.nucengdes.2005.02.004.

Salko, R., Avramova, M., Wysocki, A., Hizoum, B., Hu, J., Jambrina, A., 2023a. CTF Theory Manual: Version 4.4. Technical Report ORNL/SPR-2023/3125. Oak Ridge National Laboratory.

Salko, R., Wysocki, A., Blyth, T., Toptan, A., Hu, J., Kumar, V., Dances, C., Dawn, W., Sung, Y., Kucukboyaci, V., Gurecky, W., Lange, T., Zhao, X., Rader, J., Jernigan, C., Collins, B., Avramova, M., Magedanz, J., Palmtag, S., Clarno, K., Kropaczek, D., Hizoum, B., Godfrey, A., Pointer, D.,

Turner, J., Sankaran, R., Schmidt, R., Hooper, R., Bartlett, R., Baird, M., Pilch, M., 2022. Ctf: A modernized, production-level, thermal hydraulic solver for the solution of industry-relevant challenge problems in pressurized water reactors. Nuclear Engineering and Design 397, 111927. URL: https://www.sciencedirect.com/science/article/pii/S0029549322002783, doi:https://doi.org/10.1016/j.nucengdes.2022.111927.

Salko, R., Wysocki, A., Hizoum, B., Capps, N., 2023b. Assessment and testing of ctf for loca reflood conditions, in: NURETH-20, Washington, D.C., August 20–25, 2023, pp. 5555–5568.

Salko, R., Wysocki, A., Hizoum, B., Capps, N., 2023c. Comparison between Pin-by-Pin Subchannel and System Level Thermal Hydraulic Results for High Burnup Loss-of-Coolant Applications. Technical Report ORNL/SPR-2023/3025. Oak Ridge National Laboratory.

Salko, R., Wysocki, A., Hizoum, B., Capps, N., 2024 (in press). Assessment of ctf for modeling a loss-of-coolant accident reflood transient. Annals of Nuclear Energy .

Shaw, R., Larson, T., Dimenna, R., 1988. Development of a phenomena identification and ranking table (PIRT) for thermal-hydraulic phenomena during a PWR LBLOCA. Technical Report NUREG/CR-5074. United States Nuclear Regulatory Commission.

Thurgood, M.J., Kelly, J.M., Guidotti, T.E., Kohrt, R.J., Crowell, K.R., 1982. COBRA/TRAC - A Thermal-Hydraulic Code for Transient Analysis of Nuclear Reactor Vessels and Primary Coolant Systems: Equations and Constitutive Models. Technical Report NUREG/CR-3046. Pacific Northwest Laboratory.

Young, M., Bajorek, S., Nissley, M., Hochreiter, L., 1998. Application of code scaling applicability and uncertainty methodology to the large break loss of coolant. Nuclear Engineering and Design 186, 39–52. URL: https://www.sciencedirect.com/science/article/pii/S0029549398002179, doi:https://doi.org/10.1016/S0029-5493(98)00217-9.